An analytical electron microscopy study of pyroxene-to-pyroxenoid reactions

KENNETH J. T. LIVI, DAVID R. VEBLEN

Department of Earth and Planetary Sciences, The Johns Hopkins University, Baltimore, Maryland 21218, U.S.A.

ABSTRACT

Two occurrences of johannsenite partially altered to pyroxenoid minerals were studied by X-ray emission analytical electron microscopy in the context of the pyroxene-wollastonite polysomatic series in order to determine the relationships between composition and structure during the reactions. The complete reaction from johannsenite to rhodonite occurs in a stepwise fashion in both composition and structure. The intermediate product is a metastable mixture of rhodonite and pyroxmangite with high-Ca concentrations and with pyroxene and wollastonite polysomatic slab proportions intermediate between those of johannsenite and rhodonite. The Ca contents exceed the octahedral site occupancy limits of one-seventh and one-fifth normally observed for pyroxmangite and rhodonite, respectively. The compositions of the intermediate rhodonite and pyroxmangite are identical within analytical error, which may indicate that the pyroxene slabs in this pyroxmangite structure are more Ca rich than those of the rhodonite. This high-Ca pyroxmangite might also be viewed as a mixture of alternative slabs similar to structural slabs that occur in johannsenite and rhodonite. The M2 site of johannsenite remains rich in Ca until it reacts to the pyroxenoids, and fine-scale intergrowths of johannsenite and the pyroxenoids thus have compositions that are linear combinations of the johannsenite and pyroxenoid compositions.

The end products of two geometrically distinct solid-state reaction mechanisms, lamellar and bulk, yield pyroxenoids having the same compositions within analytical error. Dissolution of these topotactic products and reprecipitation produce unoriented, gemmy pink rhodonite with lower and presumably equilibrium Ca contents. Therefore, the polysomatic slabs change in composition during the reactions.

Late-stage alteration reactions produce several products: (1) mixed double- and triple-chain silicates that replace the pyroxene and pyroxenoids in orientations typical of amphiboles replacing pyroxenes, (2) fine-grained quartz, (3) amorphous material, and (4) carbonates. These products may be produced by either decreasing temperature or increasing X_{CO_2} and indicate that complex variations in metasomatic fluid chemistry may have occurred during alteration.

INTRODUCTION

The polysomatic model of Thompson (1978) has been used successfully to simplify complex structural relationships among many minerals and materials. Polysomatic structures are constructed by interleaving structurally and compositionally distinct slab modules, and a group of structures built from the same set of modules is called a polysomatic series (see Veblen, 1991, for review). In addition, the polysomatic model constrains the stoichiometry (as defined by structural formulae written in terms of crystallographic sites) of members of a polysomatic series to be collinear, a fact exploited by Thompson (1981) to reduce the number of components required to describe a chemical system. Furthermore, if analogous crystallographic sites possess identical site occupancies throughout the polysomatic series, then the detailed chemical compositions will also be collinear. Such compositional collinearity is observed in the ferromagnesian biopyribole

series (Veblen, 1981, 1991), where, within error, the M (mica) slabs have the same compositions in coexisting anthophyllite, jimthompsonite, chesterite, and talc as do the P (pyroxene) slabs. However, this chemical collinearity of coexisting polysomes has not been demonstrated in other polysomatic series.

In this paper, we explore the relationships between structure and composition of intergrown chain silicates that were produced by alteration of the calcium manganese clinopyroxene johannsenite to both disordered and ordered Mn-rich pyroxenoids. The pyroxene-pyroxenoid polysomatic series is based on the stacking of pyroxene-like (P) and wollastonite-like (W) structural slabs parallel to $(11\bar{1})$ of pyroxene and includes the Mn-rich pyroxenoid minerals rhodonite (PW) and pyroxmangite (PPW) (Thompson, 1978; Angel and Burnham, 1991; Veblen, 1991). Structural aspects of manganese pyroxenoids and the orientation relationships and mechanisms involved in pyroxene-to-pyroxenoid reactions have been studied

by Ohashi and Finger (1975), Koto et al. (1976), Takéuchi (1977), Takéuchi and Koto (1977), Narita et al. (1977), Czank and Liebau (1980), Angel et al. (1984), Ried (1984), Veblen (1985), Angel (1986), and Pinckney and Burnham (1988a, 1988b).

Idealized composition relationships among members of the Ca-Mn series of pyroxenes and pyroxenoids are illustrated in Figure 1, where the proportion of Ca in the octahedral sites is plotted against the proportion of P slabs in each structure. Here it is assumed that the maximum amount of Ca, given as the molar Ca/(Ca + Mn + Fe + Mg) ratio, is one-seventh in pyroxmangite and one-fifth in rhodonite. These compositional "limits" have been observed in natural samples (Ohashi et al., 1975), and the greater amount of Ca in the rhodonite of Figure 1 is consistent with natural occurrences where rhodonite and pyroxmangite coexist and with experimental phase relations in the $(Mn,Ca)SiO_3$ system (Momoi, 1974). Historically, the limits of one-seventh and one-fifth were attributed to the assumption that only one of the seven octahedral sites in pyroxmangite (M7) and only one of the five octahedral sites in rhodonite (M5) could be occupied by Ca. Figure 1 shows that if pyroxmangite and rhodonite do, in fact, contain these supposed maximum Ca contents, then a linear relationship between structure [i.e., the P/(P + W) ratio] and composition does not exist among johannsenite, rhodonite, and pyroxmangite or among wollastonite, rhodonite, pyroxmangite, and the Ca-free manganese pyroxene kanoite. However, Burnham (1971) showed that Ca probably occurs in multiple M sites of pyroxferroite, and structure refinements suggest that the same is true of pyroxmangite and perhaps of rhodonite (Ohashi and Finger, 1975; Pinckney and Burnham, 1988a). It is thus likely that the observed Ca/(Ca + Mn + Fe + Mg) limits are not structurally imposed but instead result from chemical equilibria involving other coexisting phases (Ohashi et al., 1975).

The combined use of X-ray emission analytical electron microscopy (AEM) and high-resolution transmission electron microscopy (HRTEM) allows direct correlation between structure and composition of polysomatic structures, even when structurally disordered or finely intergrown. In the present study, we have applied AEM and HRTEM to samples where johannsenite is observed to have been altered to pyroxenoids by at least three different reaction mechanisms (Veblen, 1985): (1) a topotactic lamellar mechanism involving unit-cell by unit-cell replacement of johannsenite by rhodonite and pyroxmangite, (2) a topotactic bulk mechanism involving movement of a reaction front through the original johannsenite crystal, and (3) a dissolution-reprecipitation mechanism involving the dissolution of johannsenite, rhodonite, and pyroxmangite accompanied by the crystallization of less-defective rhodonite having no fixed orientation relationship with the reactants.

The aim of this study was to answer several questions about reactions in Mn-rich chain silicates in particular and thus to learn more about reactions and crystal chem-
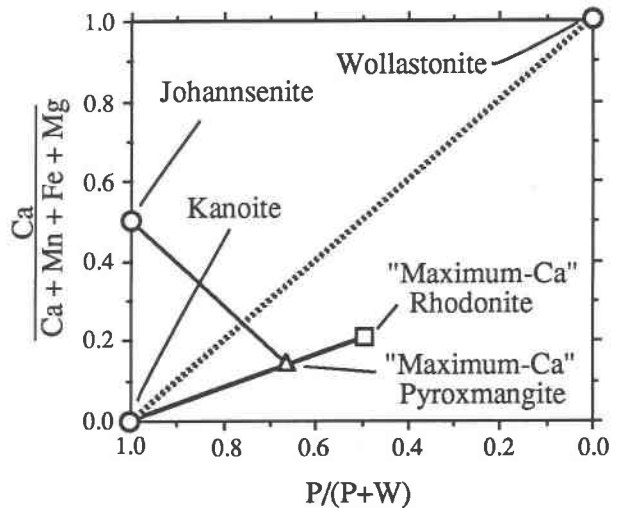

Fig. 1. Ideal Ca contents of pyroxenes and pyroxenoids vs. P and W modular proportions. "Maximum-Ca" pyroxmangite and rhodonite indicate the Ca limits that are imposed if only one-seventh and one-fifth of the M sites can be occupied by Ca in these pyroxenoids.

istry of polysomatic structures in general. (1) Do the compositions of the solid reactant and products follow the idealized compositional relationships between johannsenite, pyroxmangite, and rhodonite suggested by Figure 1, or do the compositions follow a linear trend predicted by a simple polysomatic model that assumes equal partitioning of cations in analogous cation sites of a P or W slab, regardless of the structure in which the slab is located? (2) Do the rhodonite and pyroxmangite structures partition cations in the same way when finely intergrown as when they occur in larger, well-ordered crystals? (3) Do the compositional relationships among reactant and product polysomes depend upon the structural mechanism of the reaction? (4) Is the reaction to manganese pyroxenoids preceded by a leaching of Ca from the johannsenite, or does the johannsenite maintain its initial high-Ca composition until it reacts to the pyroxenoid structures? Similarly, do the pyroxenoid reaction products possess equilibrium compositions, or are they compositionally metastable? (5) What is the nature of the late-stage alteration reactions that occur subsequent to the replacement of johannsenite by manganese pyroxenoids?

SAMPLE DESCRIPTIONS AND EXPERIMENTAL TECHNIQUES

The Rhodope Mountains sample, described by Stoinova and Pirov (1974) and Veblen (1985), contains sprays of johannsenite crystals that have partially reacted to manganese pyroxenoids and that terminate at zones consisting of dark, fine-grained mixtures of pyroxenoids, carbonates, Fe oxides, and quartz (see Veblen, 1985, Fig. 1). Large crystals (~1 mm) of gemmy pink rhodonite occur at the tips of johannsenite sprays. The second sample, EM-9 from the Empire mine as described by Abrecht
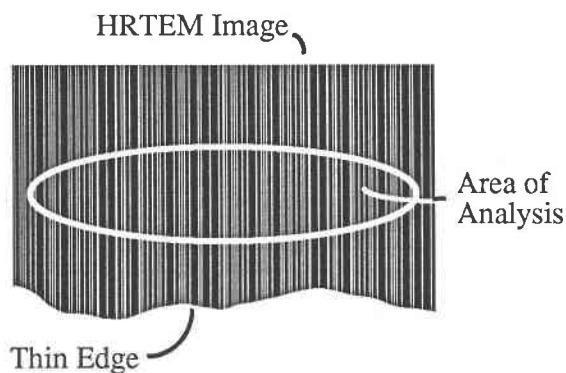
HRTEM Image

Area of Analysis

Thin Edge

Fig. 2. Schematic diagram illustrating the method of correlating the proportions of intergrown structures with AEM analyses. The width of the vertical lines represents the width of lattice fringes and is the feature used to distinguish intergrown minerals.

(1985), also consists of finely intergrown johannsenite and pyroxenoids. However, the dark, fine-grained regions and gemmy pink rhodonite crystals found in the Rhodope Mountains sample are absent in our sample of EM-9.

Samples were prepared by ion milling, and HRTEM and AEM were performed with a Philips 420T microscope equipped with an EDAX energy-dispersive X-ray detector and a Princeton Gamma-Tech System IV analyzer. Detailed procedures are given by Veblen and Bish (1988) and Livi and Veblen (1987a). For obtaining the AEM analyses, the electron beam was elongated to form an ellipse with a high aspect ratio by destigmating the second condenser lens. HRTEM images were interpreted as in Veblen (1985). Wavelength-dispersive electron microprobe (EMP) analysis was performed using a JEOL 8600 Superprobe operating at 15 keV and a beam current of 20 nA. Natural mineral standards from the Smithsonian Institution and the American Museum of Natural History were used (albite AMNH9415, orthoclase AMNHG42981, enstatite AMNH49033, rhodonite AMNH41522, fayalite AMNH10927, anorthite USNM13704), and analyses were reduced using a ZAF routine supplied by Tracor Northern.

To correlate structure and composition, HRTEM and AEM data were obtained from the same sample areas, but not in the same orientation. Because the sample orientation necessary for HRTEM imaging is also an optimum orientation for electron channeling–enhanced X-ray emission, which can cause analytical errors (Goldstein et al., 1986, p. 147), and because the sample must be tilted toward the detector to optimize collection of the X-rays, HRTEM and AEM analyses must be obtained with the specimen in two different orientations. However, care was taken to match the position of the image and the area of analysis. The volume proportions of johannsenite, pyroxmangite, rhodonite, and pyroxenoid units with more than two P slabs between W slabs were estimated by counting the numbers of fringes corresponding to each structure found in the area of the AEM analysis.

Figure 2 is a schematic diagram illustrating this technique.

RESULTS

### AEM of johannsenite and reaction products

Representative AEM analyses of johannsenite, recrystallized rhodonite, and mixed intergrowths of pyroxmangite and rhodonite for the two samples are given in Table 1, along with average EMP analyses. The AEM data are plotted in terms of $MnSiO_3-CaSiO_3-(Fe,Mg)SiO_3$ in Figure 3. The bulk and lamellar reaction products span a range of compositions from the johannsenite-rhodonite fields of Abrecht and Peters (1975), with many falling within the bustamite field and bustamite-rhodonite miscibility gap of Abrecht and Peters (1980), assuming $T = 550$ °C. In practice, identification of the reaction process responsible for any particular pyroxenoid intergrowth is impossible without images of the reaction interface. Incomplete reactions proceeding by means of the lamellar mechanism were easily identified by their texture. However, the bulk reaction mechanism produces regions of disordered pyroxenoids that are indistinguishable in appearance from complete lamellar reactions. No bulk reaction fronts were observed in either sample in this study, yet they are known to exist in the Rhodope Mountains (Veblen, 1985). This is probably due to the fact that there is a low probability that linear reaction fronts will be properly thinned for TEM observation and that reactions may have been completed in some grains. We assume that analyses of bulk reaction products are in fact included in the data of both samples. Therefore, analyses of regions produced by an unknown process are lumped together. The AEM analyses for Rhodope Mountains mixed pyroxmangite-rhodonite intergrowths that are known to be produced by the lamellar mechanism plot on a single compositional trend in Figure 3. These data also include analyses from regions of undetermined reaction mechanism. The Empire mine data could not be classified by reaction process, but the analyses again fall on a single compositional trend parallel to the Rhodope Mountains data. We find no evidence to suggest that the bulk and lamellar reaction mechanisms produce chemically distinct products. This is in contrast to the gemmy pink rhodonite produced by dissolution and reprecipitation in the Rhodope Mountains sample, which contains somewhat less Ca than the other pyroxenoids.

The analyses for the topotactic pyroxmangite-rhodonite intergrowths in Table 1 are of regions that are essentially free of johannsenite lamellae and thus represent the compositions of the pure lamellar or bulk reaction products. Even though the proportions of rhodonite and pyroxmangite lamellae are dramatically different in the four analyses from the intergrowths, the compositions of these regions are identical within analytical error. Furthermore, all of the pyroxmangite-rhodonite intergrowths have high-Ca contents, with the amount of Ca in EM-9 pyroxenoids substantially exceeding the commonly observed rhodonite compositional "limit" corresponding to one-fifth of

the M sites (Ohashi et al., 1975). Indeed, all of the intergrowths from both localities exceed the expected Ca for pyroxmangite and rhodonite mixtures having one-seventh and one-fifth Ca in the M sites, respectively.

Correlation of structure and composition in lamellar and bulk reaction products

The measured proportions of the various structures included in the areas of analysis were converted into percentages of P and W slabs using the modular compositions P for $n = 2$ (johannsenite), PW for $n = 5$ (rhodonite), PPW for $n = 7$ (pyroxmangite), PPPW for $n = 9$, and so forth, where n is the chain periodicity of each slab (see Thompson, 1978). The resulting slab ratios are plotted in Figure 4 against the proportions of Ca in the octahedral sites. This diagram can be divided into two fields. Materials that plot to the right of the vertical dotted line contain only the reaction products rhodonite, pyroxmangite, and pyroxenoid with $n \geq 9$. In this region, there is no correlation between the proportion of P slabs and the amount of Ca in the area of analysis. In contrast, materials with analyses that plot to the left of the vertical dotted line in Figure 4 contain regions with remnant, unreacted johannsenite. In this portion of the plot, both samples show a linear relationship between structure and composition. However, this relationship can be explained by a simple mixture of two components with fixed compositions, the johannsenite reactant and the pyroxenoid intergrowth product. Although the two occurrences we studied have different Ca contents for the pyroxenoid reaction products, their general trends are strikingly similar.
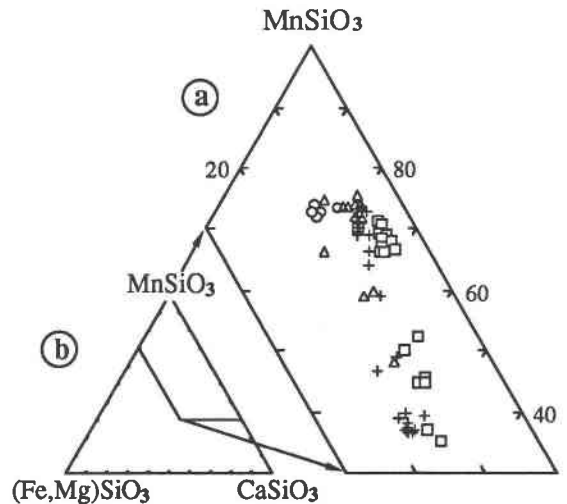
+ Rhodope Mtns., johannsenite and intergrown pyroxenes from lamellar reaction mechanism

○ Rhodope Mtns., rhodonites from dissolution-reprecipitation reaction mechanism

△ Rhodope Mtns., intergrown pyroxenes from lamellar + bulk reaction mechanisms

□ Empire Mine, johannsenite and intergrown pyroxenes from lamellar + bulk mechanisms

Fig. 3. AEM analyses plotted on a portion of the $MnSiO_3$-$(Fe,Mg)SiO_3$-$CaSiO_3$ ternary diagram (labeled a). Section b shows the full ternary diagram illustrating the portion plotted in section a.

TABLE 1. Representative AEM and EMP analyses of single-chain silicates

| | Johannsenite | | Recrystallized Rhodonite Rhodope | Mixed single-chain silicates Topotactic reaction products | | | | Average EMP analysis Rhodope Mts. | |
| | | | | Rhodope | | Empire | | | |
	Rhodope BF203	Empire EM938	Rhodope BC227	BF227	BF224	EM943	EM920	Johannsenite	Mixed single-chain silicates
Si*	1.99	2.00	1.98	1.96	1.98	1.99	1.98	1.97(0.01)§	1.98(0.01)
[4]Al	0.01	0.00	0.02	0.03	0.02	0.01	0.02	0.03(0.01)	0.01(0.003)
[6]Al	0.02	0.04	0.02	0.00	0.03	0.03	0.01	0.01(0.01)	—
Mg	0.07	0.09	0.04	0.02	0.02	0.03	0.02	0.08(0.01)	0.03(0.01)
Ti	0.00	0.00	0.00	0.00	0.00	0.00	0.01	—	—
Cr	0.01	0.00	0.00	0.01	0.00	0.01	0.01	—	—
Mn	0.75	0.73	1.47	1.47	1.41	1.31	1.37	0.70(0.08)	1.43(0.06)
Fe**	0.27	0.19	0.18	0.10	0.13	0.08	0.08	0.31(0.04)	0.16(0.05)
Ca	0.88	0.94	0.28	0.43	0.40	0.51	0.50	0.92(0.04)	0.40(0.07)
Sum	3.99	3.99	3.99	4.01	3.99	3.97	4.00	4.02	4.01
[4]Sum	2.00	2.00	2.00	1.99	2.00	2.00	2.00	2.00	1.99
[6]Sum	1.99	1.99	1.99	2.02	1.99	1.97	2.00	2.02	2.02
Ca#†	0.44	0.47	0.14	0.21	0.20	0.26	0.25	0.46	0.20
Rho%‡	0	0		91	19	81	65		
Pmg%	0	0		9	81	16	35		
Joh%	100	100	0	0	0	3	0		
Method	AEM	AEM	AEM	AEM	AEM	AEM	AEM	EMP	EMP

* Cation proportion calculated on a basis of six O atoms.
** Fe_{tot} as Fe^{2+}.
† Ca# = Ca/(Ca + Mn + Fe + Mg).
‡ Volume proportion of rhodonite, pyroxmangite, and johannsenite in analysis area.
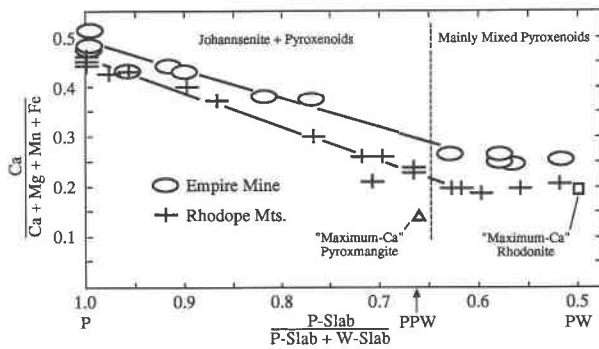§ One standard deviation of the population.

Fig. 4.   Ca in the octahedral sites vs. P-slab proportion in lamellar and bulk reaction products. Estimated analytical error is indicated by the size of the symbols. For reference, rhodonite with one-fifth M site filled (square) and pyroxmangite with one-seventh M site filled (triangle) are plotted. Compare with ideal partitioning in Figure 1.

TEM and AEM of late-stage reactions

In addition to the pyroxene-pyroxenoid reactions, both samples contain evidence of late-stage reactions, by which both remaining johannsenite and pyroxenoids partially break down to various carbonate and silicate products. In the Rhodope Mountains sample, the dark, fine-grained material replacing blades of intergrown johannsenite and pyroxenoid was found to consist of (1) quartz, (2) calcite, (3) rhodochrosite, (4) disordered, Mn-rich, unit-cell-scale mixtures of amphibole and triple-chain silicate, similar to the disordered manganese magnesium amphiboles of Maresch and Czank (1983, 1988) but with substantial Fe and Ca, and (5) a poorly crystalline material (see Fig. 5 and Table 2). A high degree of structural disorder causes severe streaking of diffraction patterns from both the reactants and the mixed-chain silicate (Fig. 6). Therefore, only one-dimensional orientation relationships could be established between them. In most cases, c^* of the single-chain silicate reactant is oriented approximately 60° from b^* of the disordered, Mn-rich pyribole product. This, coupled with HRTEM observations of fault orientations, is consistent with the conclusion that the silicate chains of the double- and triple-chain pyribole are parallel to the chains of the intergrown single-chain silicates, as is typical of amphiboles replacing pyroxenes (Veblen and Buseck, 1980). Nearly half of the pyribole analyses in Table 2 have octahedral cation sums greater than seven cations. The reason for this is unknown but may be caused by
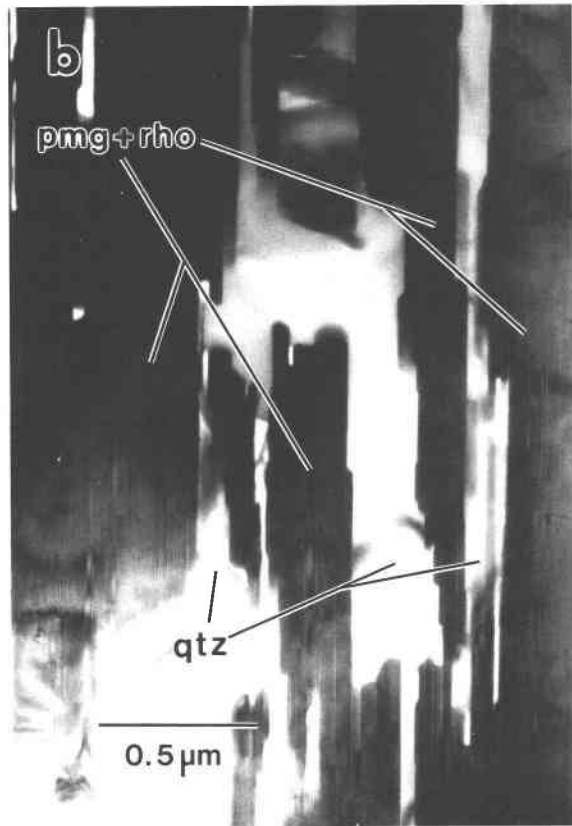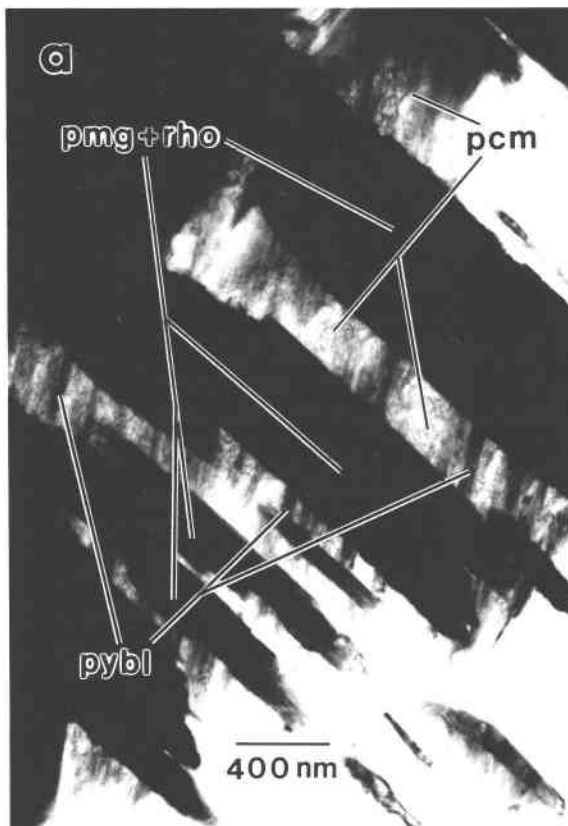

Fig. 5.   (a) Low-magnification bright-field TEM image of single-chain silicates (pmg + rho) partially replaced by mixed double- and triple-chain silicate (pybl) and poorly crystalline material (pcm) in the Rhodope Mountains sample. (b) Low-magnification bright-field TEM image of single-chain silicates partially replaced by quartz (qtz) in the Rhodope Mountains sample.

contamination of pyribole analyses with amorphous material. No consistent orientation relationships were observed between the single-chain silicates and quartz or carbonate minerals.

The texture of sample EM-9 differs from that of the Rhodope Mountains sample in that the dark, fine-grained alteration bands are missing. Instead, the late-stage reaction products are distributed throughout the thin section as groundmass. In sample EM-9, the single-chain silicates are replaced by quartz, calcite, rhodochrosite, and a poorly crystalline material, and no obvious orientation relationships were observed between reactants and products.

DISCUSSION

Structural interpretation of the AEM data

From the data plotted in Figure 4, it appears that the compositions of johannsenite, rhodonite, and pyroxmangite in these occurrences do not follow the idealized trend shown in Figure 1. They are also inconsistent with the simple notion that analogous crystallographic sites in all P modules possess the same site occupancies and that all W modules are compositionally the same; if this were the case, the relationship between Ca/(Ca + Mn + Fe + Mg) and P/(P + W) would be perfectly linear throughout Fig-
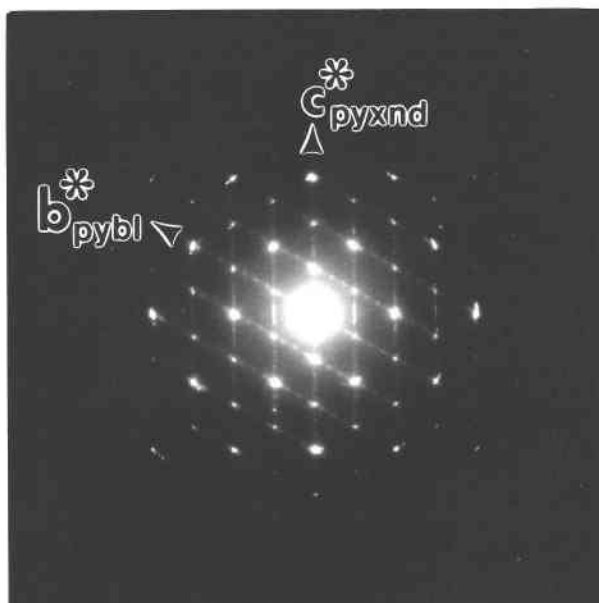

Fig. 6. Selected-area electron diffraction pattern from intergrown, disordered mixed-chain silicate (pybl) and pyroxenoids (pyxnd).

TABLE 2. AEM analyses of late-stage alteration minerals

	Mixed double- and triple-chain silicates from the Rhodope Mountains										
	BC209	BC210	BF234	BC231	BC232	BC233	BC234	BC235	BC236	BC237	BC241
Si*	7.83	7.87	7.69	7.60	7.89	7.67	7.87	7.79	7.76	7.85	7.97
[4]Al	0.17	0.13	0.29	0.40	0.11	0.33	0.13	0.21	0.20	0.15	0.03
[6]Al	0.05	0.10	0.00	0.01	0.18	0.00	0.04	0.02	0.00	0.09	0.23
Mg	3.77	3.77	2.77	1.78	1.68	1.67	2.59	1.60	1.99	2.31	2.64
Ti	0.02	0.00	0.00	0.00	0.00	0.00	0.00	0.00	0.00	0.00	0.00
Cr	0.01	0.00	0.00	0.00	0.01	0.00	0.00	0.00	0.00	0.01	0.01
Mn	1.02	0.97	1.75	1.37	1.23	1.29	2.05	1.12	2.34	1.94	1.60
Fe**	1.92	1.92	2.05	2.29	2.19	2.36	2.06	2.41	2.55	2.43	2.20
Na	0.00	0.00	0.00	0.01	0.00	0.01	0.00	0.00	0.00	0.00	0.01
K	0.04	0.04	0.00	0.05	0.03	0.03	0.00	0.02	0.03	0.03	0.02
Ca	0.22	0.25	0.62	1.70	1.66	1.82	0.31	1.98	0.29	0.24	0.19
Sum	15.05	15.05	15.17	15.21	14.98	15.18	15.05	15.15	15.22	15.05	14.90
[4]Sum	8.00	8.00	7.98	8.00	8.00	8.00	8.00	8.00	7.96	8.00	8.00
[6]Sum	7.05	7.05	7.19	7.21	6.98	7.18	7.05	7.15	7.26	7.05	6.90

	Amorphous sheets				Carbonates		
	Rhodope		Empire		Rhodope		Empire
	BC221	BC230	EM933	EM934	BF236	BC224	EM931
Si†	0.337	0.349	0.351	0.347			
Al	0.007	0.013	0.008	0.006			
Mg	0.033	0.109	0.139	0.124	0.03	0.00	0.00
Ti	0.000	0.000	0.000	0.000			
Cr	0.002	0.000	0.000	0.000			
Mn	0.197	0.104	0.030	0.037	0.18	0.33	0.06
Fe*	0.043	0.050	0.009	0.100	0.03	0.01	0.02
Na	0.000	0.000	0.000	0.000			
K	0.003	0.005	0.000	0.000			
Ca	0.038	0.017	0.002	0.035	0.76	0.65	0.93

* Cation proportion calculated on the basis of 23 O atoms.
** Fe_{tot} as Fe^{2+}.
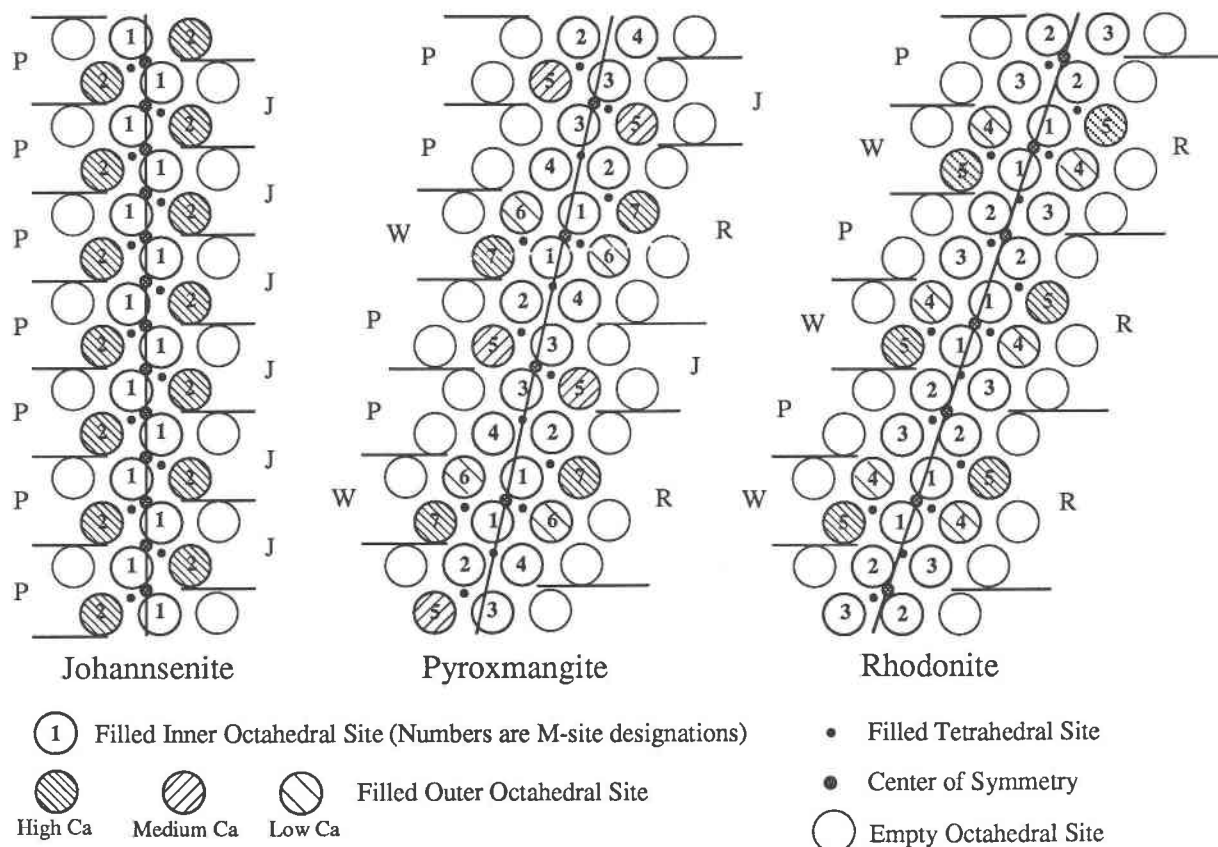† Cation proportion calculated on the basis of 1 O atom.

Fig. 7. Idealized diagram showing the arrangement of M crystallographic sites in the octahedral strips of johannsenite, pyroxmangite, and rhodonite. The P and W polysomatic slabs are shown, as are an alternative choice of slabs, J and R (see text). The Ca-bearing sites are shaded to distinguish different Ca contents.

ure 4. Indeed, the P modules of johannsenite are obviously Ca rich, but crystallographic data (see below) indicate that the P modules in normal rhodonite and pyroxmangite are relatively Ca poor, whereas the W modules are Ca rich.

The data shown in Figure 4 suggest that the rhodonite-pyroxmangite mixtures to the right of the dotted line are chemically indistinguishable, whereas a linear relationship exists between Ca contents and the amount of johannsenite present to the left of this line. Although a full and rigorous understanding of these trends would require refinement of site occupancies, which is not feasible in structurally disordered and finely intergrown materials such as these, we can speculate on their causes.

Intergrown pyroxenoid region. In regions of intergrown pyroxenoids (i.e., no remnant johannsenite), the bulk chemical composition appears to be constant for each of the two occurrences and hence independent of structure (Fig. 4). This has two major implications. (1) The coexisting pyroxmangite and rhodonite structures are compositionally identical within our analytical error. Since these structures have different P/(P + W) ratios, this could imply that either their analogous polysomatic slabs have different site occupancies or the P and W slabs have the

same composition. (2) Since the pyroxenoids at different analysis areas were intergrown on different scales, the constant composition suggests that the partitioning behavior of these structures is not grossly affected by the scale of polysomatic structural disorder.

Crystal structure refinements (Burnham, 1971; Ohashi and Finger, 1975; Pinckney and Burnham, 1988a) and typical low-Ca compositions of pyroxmangite and rhodonite show that the P modules of these pyroxenoids are usually Ca poor, whereas the sites highest in Ca are in the W slabs. Pyroxmangite (PPW) can therefore be expected to be lower in Ca than rhodonite (PW), as is normally observed (Ohashi et al., 1975; Momoi, 1974), because it has a higher P/(P + W) ratio. The X-ray diffraction data suggest that in pyroxmangite Ca is partitioned in the sequence M7 (W slab) > M5 (P slab) > M6 (W slab), with no Ca entering M1 through M4. In rhodonite, Ca appears to be largely restricted to only one site in the W slab, M5, though small amounts may also enter M4 of the W slab. The positions of the M sites on the octahedral strips are shown schematically in Figure 7.

Therefore, in the relatively high-Ca intergrown pyroxenoids from the Rhodope Mountains and Empire mine, it is most likely that significant Ca enters M5 in the py-

roxmangite, creating P slabs that are richer in Ca than those in the rhodonite. Indeed, the very high Ca/(Ca + Mn + Fe + Mg) $\cong$ 0.25 in the Empire mine pyroxenoids requires that at least 0.75 Ca atoms must enter M5 or M6, even if M7 is completely filled with Ca, and it is likely that most of it occupies M5.

Another way of viewing the Ca partitioning in the pyroxmangite and rhodonite is to slice their structures into an alternative set of slabs, a rhodonite slab and a johannsenite slab. Such a procedure is common in other polysomatic series. For example, in biopyriboles it is common to work with double-chain and triple-chain slabs rather than with the (010) M and P polysomatic slabs (e.g., Veblen and Buseck, 1979). Similarly, in disordered mixed-layer sheet silicates, for some purposes it is more convenient to use nonconventional slabs centered on the octahedral sheets (Veblen, 1983) rather than the conventional 1:1 and 2:1 layers or the polysomatic slabs of Thompson (1978). In the present case, we can define rhodonite slabs, R, each of which consists of a Thompson W slab plus two half-P slabs, as shown in Figure 7. Similarly, johannsenite slabs, J, are defined as P slabs displaced by one-half unit cell. Using these alternative slabs, rhodonite (R) then consists entirely of R slabs; johannsenite (J) is all J slabs; and pyroxmangite (RJ) contains alternating R and J slabs.

When viewed in this way, it is clear that M sites in the R slab of pyroxmangite partition Ca in much the same way as the analogous sites in the R slab of rhodonite, as shown in Figure 7. Ca is strongly concentrated in the analogous $M7_{Pmg}$ and $M5_{Rho}$, with much smaller amounts possibly entering $M6_{Pmg}$. Because of its similarity to the $M6_{Pmg}$ site, $M4_{Rho}$ may also contain limited amounts of Ca, although no refinement data substantiate this. The other sites are Ca free. In our high-Ca samples, Ca is also apparently partitioned into the M5 sites in the J slab of pyroxmangite, which are analogous to the M2 sites of the J slab in johannsenite (Fig. 7). In pyroxmangite occurrences with lower Ca, the R slabs of pyroxmangite may be similar in their cation-partitioning behavior to the R slabs of rhodonite, whereas the J slabs are depleted in Ca and resemble more the analogous slabs in $MnSiO_3$ clinopyroxene. Indeed, Angel and Burnham (1991) and Veblen (1991) compared the structure of the P slabs in low-Ca pyroxmangite with those of $MnSiO_3$ clinopyroxene and johannsenite. Although all three structures are similar, it appears that the pyroxene-like region of low-Ca pyroxmangite is more similar in structure to that of $MnSiO_3$ clinopyroxene than it is to that of high-Ca johannsenite.

Johannsenite + pyroxenoids region. The linear relationship between composition and structure exhibited by both samples in regions containing both johannsenite and pyroxenoids clearly does not result from the P and W slabs having the same compositions in both the pyroxene and the pyroxenoids; although the M5 sites of the pyroxmangite may contain more Ca than is normal, they probably do not have Ca occupancies close to 1.0, as is the

case with the johannsenite M2 sites. Instead, the linear relationship appears to represent a simple mixing line between the very Ca-rich johannsenite samples and the mixed pyroxenoids (with an average P/P + W ratio of approximately 0.6). This mixing line suggests that the johannsenite maintains its high-Ca composition until the reaction occurs, i.e., Ca is not leached from the pyroxene prior to conversion to the pyroxenoid structures. This is consistent with the notion that all of the diffusion necessary for the reaction occurs along defects or interfaces at the exact reaction sites rather than by bulk diffusion through the structure (see Veblen, 1991, for a discussion of diffusion in polysomatic reactions).

Composition and stability of the different pyroxenoid types

Dependence of chemistry on reaction mechanism. The AEM data provide no evidence for a chemical distinction between the intergrown pyroxenoids produced by the lamellar reaction mechanism and those produced by the bulk mechanism involving an advancing reaction front (Table 1 and Fig. 3). This may be because the reactant is the same in both cases and the product is similar (disordered intergrown rhodonite and pyroxmangite lamellae), so that the cation partitioning between reactant and products is also similar. In contrast, the late-stage gemmy pink rhodonite in the Rhodope Mountains sample, which appears to have formed by a nontopotactic, dissolution-precipitation mechanism, is substantially lower in Ca than the topotactic reaction products. This chemical difference may be related to the different reaction mechanism or to the rate and timing of reaction.

Ca contents and thermodynamic stability. As noted above, the intergrown pyroxenoids that form by topotactic reactions have very high-Ca contents. Based upon observations from both natural and synthetic systems (Abrecht and Peters, 1980), the compositions of the rhodonite and the pyroxmangite, especially in sample EM-9, lie well within the rhodonite-bustamite and rhodonite-johannsenite miscibility gaps and are hence metastable. In contrast, the gemmy pink rhodonite that replaces this metastable intermediate-reaction product in the Rhodope Mountains sample is relatively low in Ca and may represent a stable rhodonite composition. Thus, this occurrence provides an example of the Ostwald step rule, which states that "in all processes it is not the stablest state with the least amount of free energy which is initially obtained, but the least stable lying nearest to the original state in free energy" (Ostwald, 1897; Verma and Krishna, 1966, p. 21).

Comparison of AEM and EMPA data. The pyroxenoid analyses for sample EM-9 presented in Table 1 and Figure 3 are similar to those obtained by Abrecht (1985) using EMP analyses. Because his analyses show anomalously high Ca for pyroxenoids, Abrecht reached the logical conclusion that his analysis spots probably contained submicroscopic lamellae of johannsenite intermixed with rhodonite. The AEM analyses show, however, that even

TABLE 3. Isovolumetric mass balance for pyroxene-pryroxenoid reactions

	Rhodope Mountains isovolumetric reactions				Empire mine isovolumetric reactions			
	2.472Joh → 1.000Rho		3.426Joh → 1.000Pmg		2.472Joh → 1.000Rho		3.426Joh → 1.000Pmg	
	Δ*	% change**	Δ	% change	Δ	% change	Δ	% change
Si	0.09	−0.5	−0.45	2.3	−0.01	0.0	−0.45	2.3
Al	−0.003	1.0	−0.29	96.3	0.10	−31.9	−0.01	3.9
Mg	0.49	−71.4	0.68	−98.5	0.69	−100.1	0.81	−117.9
Ca	4.41	−50.6	6.46	−74.2	4.20	−48.2	5.74	−65.9
Mn	−7.28	98.1	−9.46	127.5	−6.48	87.3	−8.33	112.3
Fe	1.67	−62.6	1.88	−70.4	1.08	−40.5	1.48	−55.6
O	−0.62	1.0	−1.77	3.0	−0.62	1.0	−1.77	3.0

  * No. of moles liberated (+) or consumed (−).
  ** Percent change of no. of moles in solid.

pyroxene-free regions can possess these abnormally high-Ca compositions. Future EMPA studies should thus take into account the observation that the manganese pyroxenoid structures can, at least in some circumstances, accommodate large amounts of Ca metastably.

Mass balance for the johannsenite-pyroxenoid reactions. Observations of the terminations of pyroxenoid lamellae formed during the lamellar reactions suggest that the johannsenite-to-pyroxenoid reactions in the Rhodope Mountains and Empire mine occurrences are isovolumetric (Veblen, 1985; Livi and Veblen, 1987b). This conclusion is based on the fact that the growing lamellae do not observably deform the surrounding pyroxene at their tips; such deformation would be apparent for a volume change of more than a few percent. Table 3 shows mass balances for the pyroxene-pyroxenoid reactions in both occurrences, calculated using the $\Delta V/\overline{V}^0_{\mathrm{Joh}} = 0$ constraint. Not surprisingly, the reactions in both samples are similar. Major amounts of Mn are introduced, with large amounts of Ca and some Fe and Mg being liberated to the metasomatic fluid. At least some of the Ca, Fe, and Mg may have played a role in the late-stage alteration reactions.

Late-stage reactions

Ideally, the sequence of reactions in our samples should be explicable in terms of phase relations developed in previous studies of Mn-rich metasomatic rocks (e.g., Abrecht, 1980, 1985; Abrecht and Peters, 1980; Allen and Fahey, 1953, 1957; Peters et al., 1978; Rose and Burt, 1979). For example, the late-stage reaction products (quartz, rhodochrosite, calcite, poorly crystallized material, and disordered Mn-rich pyriboles) should be interpretable as resulting from changing Mn and Ca activities in the metamorphic fluid combined with either decreasing temperature or changes in the activity of CO_2. To illustrate possible responses to temperature, two trajectories are shown in the T-X_{Ca} diagram of Figure 8. Trajectory 1 predicts mixtures of rhodonite and johannsenite. Instead, in this study, we observe that the first products formed are disordered intergrowths of high-Ca rhodonite and pyroxmangite, mixed with johannsenite, which underscores the metastable character of this reaction. With more rapid changes in temperature (trajectory 2 in Fig.

8), calcite and then rhodochrosite along with quartz would be produced at the expense of the single-chain silicates. Alternatively, simple increases in the activity of CO_2 would stabilize the carbonates over single-chain silicates (see Abrecht and Peters, 1980, their Fig. 9a).

The formation of metastable disordered pyroxenoids, which in one occurrence are then replaced by a more normal law-abiding rhodonite, followed by the precipitation of both rhodochrosite and calcite, underscores the complex alteration history in these Mn-rich skarns. A single trajectory on the T-X diagram of Figure 8 cannot simply account for all of the observed textures and phase assemblages, which possibly suggests complex variations in fluid chemistry during cooling. Furthermore, the observed disordered Mn-rich biopyriboles and poorly crystallized gel-like materials are not accounted for by phase diagrams such as that in Figure 8. Like the high-Ca intergrown pyroxenoids, these phases may well be metastable.

CONCLUSIONS

By combining AEM compositional information and HRTEM structural data obtained from the same sample areas, we have shown that the compositional relationships resulting from the reaction of johannsenite to Mn-rich pyroxenoids are not consistent with the assumption that Ca can occupy only one-seventh of the octahedral sites in pyroxmangite and one-fifth of the octahedral sites in rhodonite. The data are also inconsistent with the hypothesis that analogous polysomatic slabs must partition cations in identical fashion throughout a polysomatic series, although such a relationship does seem to exist among ferromagnesian biopyriboles with different chain widths. Instead, the data are consistent with a pyroxmangite structure with a relatively high-Ca occupancy of the M5 sites, producing a structural slab that is similar to analogous slabs in johannsenite. The very high-Ca contents of pyroxmangite and rhodonite produced by reaction from johannsenite are almost certainly metastable, and, in one of the two occurrences we examined, the metastable pyroxenoid was subsequently replaced by a more stable and relatively well-ordered lower-Ca rhodonite.

The combined AEM and HRTEM results also reveal some of the complexities of alteration reactions in Mn-
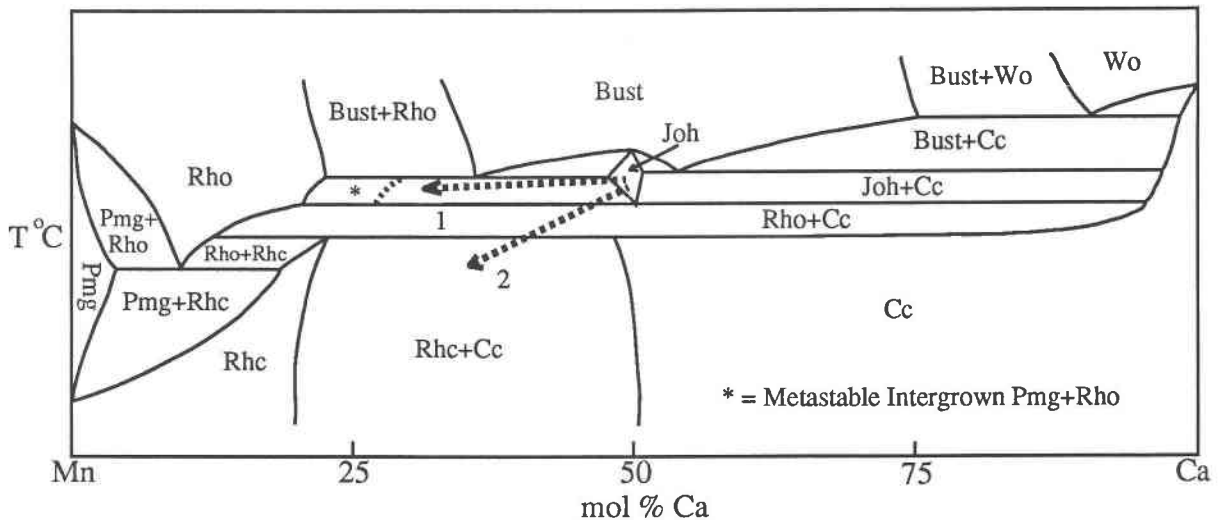
Fig. 8. An empirical T-X_{Ca} phase diagram for the system CaO-MnO-SiO_2-CO_2 (after Abrecht, 1985). Trajectories that would be expected to form intergrown rhodonite and johannsenite (1) and carbonates (2) are shown. Joh = johannsenite, Rho = rhodonite, Pmg = pyroxmangite, Bust = bustamite, Cc = calcite, Rhc = rhodochrosite, Wo = wollastonite.

rich skarns. Johannsenite appears to maintain its composition until it reacts to pyroxenoids, rather than first losing Ca to the metasomatic fluid. Intergrown pyroxenoid appears to have the same composition regardless of whether it formed by lamellar or bulk reaction mechanisms. Late-stage reactions following johannsenite-to-pyroxenoid replacement produce a variety of very fine-grained silicates and carbonates. These late-stage products cannot be simply rationalized in terms of previously presented phase relations, stressing the importance of metastability in relatively low-temperature alteration reactions.

REFERENCES CITED

Abrecht, J. (1980) Stability relations in the system $CaSiO_3$-$CaMnSi_2O_6$-$CaFeSi_2O_6$. Contributions to Mineralogy and Petrology, 74, 253–260.
——— (1985) Manganiferous pyroxenes and pyroxenoids from three Pb-Zn-Cu skarn deposits. Contributions to Mineralogy and Petrology, 89, 379–393.
Abrecht, J., and Peters, T. (1975) Hydrothermal synthesis of pyroxenoids in the system $MnSiO_3$-$CaSiO_3$ at P_f = 2kb. Contributions to Mineralogy and Petrology, 50, 241–246.
——— (1980) The miscibility gap between rhodonite and bustamite along the join $MnSiO_3$-$Ca_{0.60}Mn_{0.40}SiO_3$. Contributions to Mineralogy and Petrology, 74, 261–269.
Allen, V.T., and Fahey, J.J. (1953) Rhodonite, johannsenite, and ferroan johannsenite at Vanadium, New Mexico. American Mineralogist, 38, 883–890.
——— (1957) Some pyroxenes associated with pyrometasomatic zinc deposits in Mexico and New Mexico. Geological Society of America Bulletin, 63, 881–896.
Angel, R.J. (1986) Transformation mechanisms between single-chain silicates. American Mineralogist, 71, 1441–1454.
Angel, R.J., and Burnham, C.W. (1991) Pyroxene-pyroxenoid polysomatism revisited: A clarification. American Mineralogist, 76, 900–903.
Angel, R.J., Price, G.D., and Putnis, A. (1984) A mechanism for pyroxene-pyroxenoid and pyroxenoid-pyroxenoid transformations. Physics and Chemistry of Minerals, 10, 236–243.
Burnham, C.W. (1971) The crystal structure of pyroxferroite from Mare Tranquilitatis. Proceedings of the Second Lunar Science Conference, 1, 47–57.
Czank, M., and Liebau, F. (1980) Periodicity faults in chain silicates: A new type of planar lattice fault observed with high-resolution electron microscopy. Physics and Chemistry of Minerals, 9, 85–93.
Goldstein, J.I., Williams, D.B., and Cliff, G. (1986) Quantitative X-ray analysis. In D.C. Joy, A.D. Romig, Jr., and J.I. Goldstein, Eds., Principles of analytical electron microscopy, p. 155–217. Plenum, New York.
Koto, K., Morimoto, N., and Narita, H. (1976) Crystallographic relationships of the pyroxenes and pyroxenoids. Journal of the Japanese Association of Mineralogy, Petrology and Economic Geology, 71, 248–254.
Livi, K.J.T., and Veblen, D.R. (1987a) "Eastonite" from Easton, Pennsylvania: A mixture of phlogopite and a new form of serpentine. American Mineralogist, 72, 113–125.
——— (1987b) Analytical electron microscopy (AEM) of a pyroxene-to-pyroxenoid reaction (abs.). Eos, 68, 453.
Maresch, W.V., and Czank, M. (1983) Phase characterization of synthetic amphiboles on the join $Mn_x^{2+}Mg_{7-x}[Si_8O_{22}](OH)_2$. American Mineralogist, 68, 744–753.
——— (1988) Crystal-chemistry, growth-kinetics and phase-relationships of structurally disordered (Mn^{2+},Mg)-amphiboles. Fortschritte der Mineralogie, 66, 69–121.
Momoi, H. (1974) Hydrothermal crystallization of $MnSiO_3$ polymorphs. Mineralogical Journal, 7, 359–373.
Narita, H., Koto, K., and Morimoto, M. (1977) The crystal structures of $MnSiO_3$ polymorphs (rhodonite- and pyroxmangite-type). Mineralogical Journal, 8, 329–342.
Ohashi, Y., and Finger, L.W. (1975) Pyroxenoids: A comparison of refined structures of rhodonite and pyroxmangite. Carnegie Institution of Washington Year Book, 74, 564–569.

Ohashi, Y., Kato, A., and Matsubara, S. (1975) Pyroxenoids: A variation in chemistry of natural rhodonites and pyroxmangites. Carnegie Institution of Washington Year Book, 74, 561–564.

Ostwald, W. (1897) The formation and changes of solids. Zeitschrift für Physikalische Chemie, 22, 289–330 (in German).

Peters, T., Trommsdorff, V., and Sommerauer, J. (1978) Manganese pyroxenoids and carbonates. Critical phase relations in metamorphic assemblages from the Alps. Contributions to Mineralogy and Petrology, 66, 383–388.

Pinckney, L.R., and Burnham, C.W. (1988a) Effects of compositional variation on the crystal structures of pyroxmangite and rhodonite. American Mineralogist, 73, 798–808.

——— (1988b) High-temperature crystal structure of pyroxmangite. American Mineralogist, 73, 809–817.

Ried, H. (1984) Intergrowth of pyroxene and pyroxenoid; chain periodicity faults in pyroxene. Physics and Chemistry of Minerals, 10, 230–235.

Rose, A.W., and Burt, D.M. (1979) Hydrothermal alteration. In H.L. Barnes, Ed., Geochemistry of hydrothermal ore deposits (2nd edition), p. 173–235. Wiley, New York.

Stoinova, M., and Pirov, T. (1974) The Govedarnika polymetallic deposit, District of Luki, Northern Rhodope Mountains. In P. Dragov and B. Kolkovski, Eds., Twelve ore deposits in Bulgaria, Fourth Symposium, Varna, Bulgaria, p. 134–148. International Association on the Genesis of Ore Deposits (IAGOD), Varna, Bulgaria.

Takéuchi, Y. (1977) Designation of cation sites in pyroxenoids. Mineralogical Journal, 8, 431–438.

Takéuchi, Y., and Koto, Y. (1977) A systematics of pyroxenoid structures. Mineralogical Journal, 8, 239–249.

Thompson, J.B., Jr. (1978) Biopyriboles and polysomatic series. American Mineralogist, 63, 239–249.

——— (1981) An introduction to the mineralogy and petrology of the biopyriboles. In Mineralogical Society of America Reviews in Mineralogy, 9A, 141–188.

Veblen, D.R. (1981) Non-classical pyriboles and polysomatic reactions in biopyriboles. In Mineralogical Society of America Reviews in Mineralogy, 9A, 189–236.

——— (1983) Microstructures and mixed layering in intergrown wonesite, chlorite, talc, biotite, and kaolinite. American Mineralogist, 68, 566–580.

——— (1985) TEM study of a pyroxene-to-pyroxenoid reaction. American Mineralogist, 70, 885–901.

——— (1991) Polysomatism and polysomatic series: A review and applications. American Mineralogist, 76, 801–826.

Veblen, D.R., and Bish, D.L. (1988) TEM and X-ray study of orthopyroxene megacrysts: Microstructures and crystal chemistry. American Mineralogist, 73, 677–691.

Veblen, D.R., and Buseck, P.R. (1979) Chain-width order and disorder in biopyriboles. American Mineralogist, 64, 687–700.

——— (1980) Microstructures and reaction mechanisms in biopyriboles. American Mineralogist, 65, 599–623.

Verma, A.R., and Krishna, P. (1966) Polymorphism and polytypism in crystals. Wiley, New York.